Radboud Repository

Radboud University Nijmegen

PDF hosted at the Radboud Repository of the Radboud University Nijmegen

The following full text is a preprint version which may differ from the publisher's version.

For additional information about this publication click this link.
http://hdl.handle.net/2066/140106

Please be advised that this information was generated on 2017-12-05 and may be subject to change.

arXiv:1503.03811v1 [cond-mat.mes-hall] 12 Mar 2015

Melting temperature of graphene

J. H. Los, K.V. Zakharchenko, M. I. Katsnelson, Annalisa Fasolino*
Radboud University Nijmegen/Institute for Molecules and Materials,
Heyendaalseweg 135, 6525AJ Nijmegen, The Netherlands and
* *a.fasolino@science.ru.nl*

(Dated: March 13, 2015)

We present an approach to the melting of graphene based on nucleation theory for a first order phase transition from the 2D solid to the 3D liquid via an intermediate quasi-2D liquid. The applicability of nucleation theory, supported by the results of systematic atomistic Monte Carlo simulations, provides an intrinsic definition of the melting temperature of graphene, T_m, and allows us to determine it. We find $T_m \simeq 4510$ K, about 250 K higher than that of graphite using the same interatomic interaction model. The found melting temperature is shown to be in good agreement with the asymptotic results of melting simulations for finite disks and ribbons of graphene. Our results strongly suggest that graphene is the most refractory of all known materials.

I. INTRODUCTION

Surprisingly, understanding of melting is still an open problem in condensed matter physics. For instance, after more than hundred years, there is still no reliable theoretical justification of the Lindemann criterion [1]. Nevertheless, the melting temperature T_m is well-defined as the temperature at which the Gibbs free energy curves of the liquid and solid phase intersect. Graphene, however, is a quasi-2D crystalline membrane [2], which melts into a 3D liquid phase [3]. The different dimensionality of these two phases makes it impossible to determine their free energy difference with existing methods, so that it is a priori not even clear how to define T_m. Here we show that a 2D nucleation theory offers a way to overcome this difficulty and give a reliable quantitative value of T_m.

While for 3D systems, there is no consensus about how to describe melting and premelting anomalies, for a 2D crystal there is a commonly accepted microscopic scenario for melting [4], the KTHNY theory [5–9]. In the KTHNY theory, melting occurs via unbinding of topological defects, like vortices in superconductors [10]. This scenario seems not to apply to graphene. Apart from the embedding in 3D space, which affects all its structural and thermodynamic properties [2, 11], the nature of defects is completely different from those considered in the KTHNY theory. In graphene, there are neither observations nor predictions of stable single pentagons or heptagon defects (disclinations). Dislocations (pentagon-heptagon pairs) have been observed mainly at grain boundaries [12]. The 4.6 eV formation energy [14] of a Stone-Wales (SW) defect made of two adjacent pentagon-heptagons (57) pairs is much lower than the formation energy of two well separated 57 pairs as occurring in small angle grain boundaries [13]. In the Appendix we show how the formation energy of two 57 pairs rapidly increases with separation. The relative stability of SW defects make them play a crucial role in the premelting behavior of graphene [3] and prevents them to split into two 57 defects and further, and by this to follow the KTHNY scenario.

In ref.3 we have shown that, within the same model of interactions that we use here, spontaneous melting of graphene occurs at a temperature that we call T_m^* of 4900 K, giving an upper limit for the true melting temperature T_m of graphene. Here we show that the melting of bulk graphene can be described by nucleation theory, allowing an unambigous definition of the melting temperature, T_m. We find $T_m \simeq 4510$ K, about 250 K higher than that of graphite[16] and sofar the highest of all materials.

The paper is organized as follows. In section II we review previous results [3] on the spontaneous melting of bulk graphene. In section III we introduce an approach based on classical and kinetic nucleation theory to the melting in 2D. This approach is applied in section IV to bulk graphene. The melting of finite disks and ribbons is presented in sections V and VI respectively. Summary and conclusions are given in section VII.

II. SPONTANEOUS MELTING

In a previous work [3], we have studied the spontaneous melting of graphene by means of Monte Carlo (MC) simulations based on the reactive bond order potential LCBOPII [14]. A suitable Lindemann type order parameter for graphene was defined as $\gamma_{12} = (1/a^2) < (\mathbf{r}_i - (1/12)\sum_j \mathbf{r}_j)^2 >$, where $a = 1/\sqrt{\pi\rho}$ is the atomic radius, with ρ the 2D particle density, $\mathbf{r}_i$ is the position of the i-th atom and the sum over j runs over the 12 atoms closest to atom i. For graphene, melting starts at $\gamma_{12} \simeq 0.1$, close to the value found for a strictly 2D, triangular lattice [15] .

In Fig. 1a we show a snapshot from a MC simulation in which a bulk graphene system consisting of N =1008 atoms with periodic boundary conditions (PBCs) is heated at a constant rate. Fig. 1b and c show the potential energy E and γ_{12} as a function of the applied, increasing temperature found in 8 independent MC simulations. Melting is signalled by a jump in E and γ_{12}, but with large variations in the observed melting temperature, T_m^*, at which this jump occurs for different, independent simulations. This jump as well as the coexistence of solid and liquid parts in Fig. 1a are typical

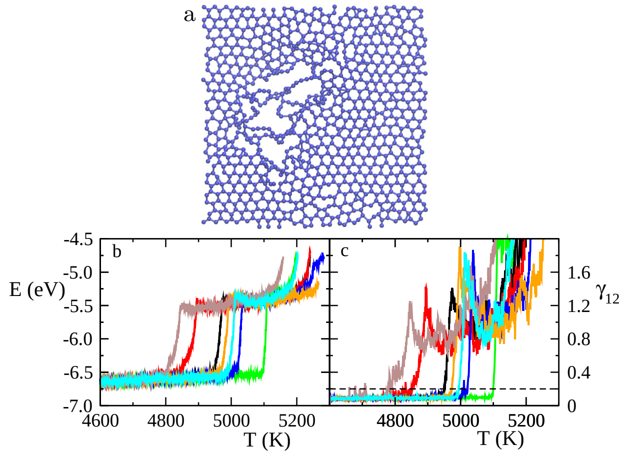

FIG. 1. a) A snapshot of simulated bulk graphene at the onset of melting. The system contains 1008 atoms with PBCs. Note the coexistence of solid and liquid parts. b) Energy E and c) and order parameter γ_{12} as a function of temperature T during a linear temperature ramp for 8 independent simulations.

features of first order phase transitions. Obviously, the lowest $T_m^* = 4900$ K found in Ref. 3 constitutes only an upper limit for the true melting temperature T_m of graphene.

III. NUCLEATION THEORY APPROACH TO MELTING IN 2D

Here we propose a quantitative approach to determine T_m by considering the melting as a process initiated and dominated by the nucleation of liquid nuclei in the solid sheet, a typical scenario for a first order phase transition. The possible applicability of nucleation theory is furthermore suggested by our observation that the melting process occurs in two steps. First the graphene sheet transforms into a sort of quasi-2D liquid phase consisting of entangled and interconnected chains remaining roughly within the quasi-2D plane of the previously solid sheet. Eventually, the chains start to disentangle and extend to 3D space, with a diverging simulation box in NPT simulation at zero pressure applied in this work. In Fig. 1 this "graphene → quasi-2D liquid → 3D liquid" scenario is reflected in the energy curve: first, at melting, the energy steeply increases by about 1.05 eV after which it remains roughly constant for a while before it starts to increase further. This two steps scenario via an intermediate quasi-2D liquid phase would imply that the melting temperature of graphene is in fact the temperature at which the 2D solid and the quasi-2D liquid phases are in equilibrium. Looking at the snapshot in Fig. 1a, it can also be argued that before complete melting, when liquid nuclei start to form in the solid sheet, the liquid phase remains connected with the solid sheet at the edges of the nucleus, constraining it to stay within quasi-2D configurations. The importance of assuming the existence of a quasi-2D liquid phase with its own thermodynamic properties is that it allows us to formulate a nucleation theory for the melting of a 2D solid embedded in 3D space, the case of graphene. If the melting can only take place via this intermediate, quasi-2D liquid phase, then this intermediate phase is decisive for the location of the melting temperature of graphene.

For the analysis of melting in terms of nucleation theory we performed two series of simulations: simulations at constant temperature and simulations applying a linear temperature ramp. To assess the accuracy of our approach, we will compare classical nucleation theory (CNT) and kinetic nucleation theory (KNT), as described hereafter. We use LCBOPII [14] for the interatomic interactions, as in Ref. [3]. We point out that the melting temperature of graphite according to LCBOPII has been accurately determined to be 4250 K [16].

For the application of CNT to melting in 2D, we write the work $W(r)$ done to form a quasi-2D liquid nucleus of radius r as:

$$W(r) = \pi r^2 \rho \Delta\mu + 2\pi r \gamma_{sl} \tag{1}$$

where $\Delta\mu = \mu_l - \mu_s$ is the chemical potential difference per particle between the quasi-2D liquid phase and the solid phase, and γ_{sl} is the solid-liquid interface free energy. Note that $\pi r^2 \rho$ is the number of liquid particles inside the nucleus, which should indeed grow as r^2 due to the 2D geometry of the solid. For $T > T_m$, $\Delta\mu < 0$ and $W(r)$ has a maximum at the critical nucleus size with radius $r_c = -\gamma_{sl}/(\rho\Delta\mu)$ equal to $W_c \equiv W(r_c) = -\pi\gamma_{sl}^2/(\rho\Delta\mu)$. Using the thermodynamic relation $\Delta\mu = \Delta h - T\Delta s \approx (\Delta h/T_m)(T_m - T)$, with Δh and $\Delta s = \Delta h/T_m$ the melting enthalpy (latent heat) and melting entropy per particle respectively, the nucleation probability is derived to be:

$$P_{nucl}^{CNT} \equiv K \exp(-\beta W_c) = K \exp\left(-\frac{\beta\, \alpha T_m}{(T - T_m)}\right) \tag{2}$$

where K is a kinetic prefactor, $\beta = 1/(k_B T)$ and we defined $\alpha \equiv \pi\gamma_{sl}^2/(\rho\Delta h)$.

If the melting is dominated by nucleation, then the average time t^* required for melting to occur is given by the solution of the equation:

$$N_{nucl}(t^*) = \int_0^{t^*} P_{nucl}^{CNT}(T(t))dt = 1 \tag{3}$$

where $N_{nucl}(t)$ is the number of (super)critical nuclei at time t. At constant temperature $T > T_m$, eq. 3 simplifies to $t^* = 1/P_{nucl}(T)$. Instead, if the system is slowly heated at a heating rate η, such that $T = T_m + \eta t$, we have to solve eq. 3 numerically for t^*. The temperature at which melting is expected, T_m^*, is then readily obtained from $T_m^* = T_m + \eta t^*$.

In principle, CNT does not specify neither the prefactor K nor its temperature dependence. Therefore, we take K constant in our simulation analysis based on CNT. Nucleation is then determined by three parameters: α, K and T_m. Expressions for the temperature dependence of the kinetic prefactor belong to the domain of kinetic nucleation theory (KNT), which allows us to perform a more accurate analysis.

The starting point of KNT [17] is quite different from that of CNT. KNT assumes a (liquid) cluster size distribution (CSD) governed by a coupled set of master equations with appropriate boundary conditions. In CNT, the CSD is proportional to $\exp(-\beta W(r))$ so that it has a minimum for clusters of the critical nucleus radius r_c, where W is maximal, while it increases exponentially beyond the critical size. The latter prediction is clearly unphysical. In KNT, this unphysical behavior is avoided by requiring the CSD to satisfy the boundary condition $X_N = 0$, where X_N is the number of clusters that incorporate all N atoms of the system. Eventually, KNT leads to a stationary state nucleation rate given by:

$$P_{nucl}^{KNT} = f_c Z \exp\left(-\frac{\beta\ \alpha T_m}{(T - T_m)}\right) \quad (4)$$

where f_c is the attachment rate for a particle to join a nucleus of the critical size, Z is the so-called Zeldovich factor and α as defined before. The attachment rate can be expressed as:

$$f_c = \nu_{ref}\frac{T}{T_{ref}} g\sqrt{n_c}\exp(-\beta E_a) \quad (5)$$

where $\nu_{ref} \simeq k_B T_{ref}/h$ (with h the Planck constant) is an attempt frequency at some reference temperature T_{ref}, which we choose to be $T_{ref} = 4500$ K, $g\sqrt{n_c}$ accounts for the number of perimeter sites around a critical nucleus with $n_c = \pi r_c^2 \rho = \pi\gamma_{sl}^2/(\rho\Delta\mu^2)$ and g a geometrical factor, while E_a is an activation energy barrier for the attachment process. For a circular nucleus, the number of perimeter sites is given by $2\pi r_c d\rho = (2d/a)\sqrt{n_c}$ where d is the width of one atomic layer (or shell), whence $g = 2d/a$. Following Ref. [17], the Zeldovich factor Z for our 2D case is found to be:

$$Z = \left(\frac{\beta}{4\pi}\frac{|\Delta\mu|^3}{\alpha\Delta h}\right)^{1/2}. \quad (6)$$

Comparing the parameters in KNT to those in CNT, and noting that $\tilde{K} \equiv \nu_{ref} g$ replaces K in CNT, there are two additional parameters: Δh and E_a. However, Δh can directly be obtained from the simulations as the melting energy (at zero pressure): $\Delta h \simeq 1.05$ eV (see Fig. 1b). The activation energy barrier E_a is typically a few eV, implying that the temperature dependence introduced by $\exp(-\beta E_a)$ is rather weak within the temperature range of interest and has only a very minor effect (as we verified). We have taken $E_a = 2.6$ eV fixed, equal to the activation energy for diffusion in a mixed sp-sp^2 carbon liquid, as found with LCBOPII [16].

LCBOPII include short range (covalent), long range (van der Waals) and middle range (MR) interactions [14]. The latter contribution is a correction that improves the reactive properties and, by construction, does not affect the equilibrium carbon structures at low T. Since many simulations were required to obtain sufficient statistics, and the use of the full potential including the MR part is computationally demanding for Molecular Dynamics (MD) simulations, we have performed MC simulations. Following Ref. 18, we then assume that time is proportional to the number of MC cycles t_{MC} (one cycle being N trial moves) so that $t = Ct_{MC}$ where C is a time calibration factor assumed to be constant within a limited temperature range provided that the acceptance rate is kept constant. To assess the validity and accuracy of this approximation, we also performed Molecular Dynamics simulations, but without the MR part of the LCBOPII for the sake of feasibility, and compared the results to those from MC simulations using the same potential (i.e. LCBOPII without the MR part). The MC and MD simulations were performed applying a linear temperature ramp. In the MD simulations the temperature was raised by using the Berendson thermostat and scaling the velocities at every time step, while in the MC simulations the temperature was raised every 5 MC cycles. We considered a series of heating rates, and for each of them the average T_m^* was determined from 48 independent simulations. For each simulation, T_m^* was determined by the intersection of the γ_{12} curve with the horizontal line at $\gamma_{12} = 0.2$ (see Fig. 1a). Plotting the average T_m^* as a function of η, a very good agreement between the MD and MC results was obtained by applying a time calibration factor equal to $C = 5.56\ 10^{-4}$ ps/cycle, as is shown in Fig. 2. We note that for the determination of T_m using nucleation theory, it is sufficient that $t = Ct_{MC}$ holds and we do not need C.

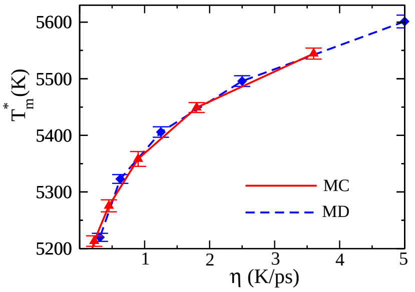

FIG. 2. Comparison of the average, observed melting temperature, T_m^*, of bulk graphene (1008 atoms with PBCs) as a function of the heating rate obtained from MD (blue diamonds) and MC (red triangles) simulations after calibration, using LCBOPII without the middle range interactions. Error bars are based on 48 independent simulations. Lines are guides to the eye.

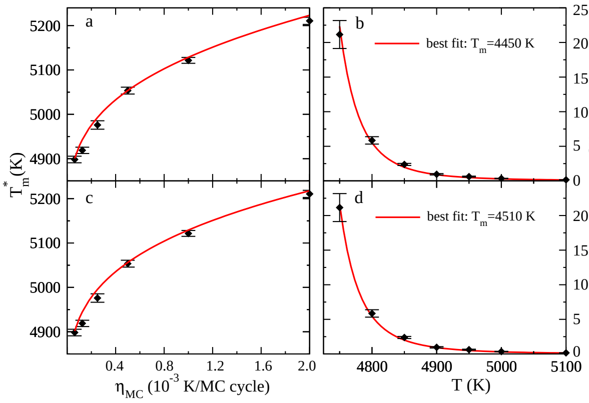

FIG. 3. Symbols: a) and c) average melting temperature T^*_m as a function of the MC heating rate η_{MC} and b) and d) MC 'time' t^*_{MC} required for melting at isothermal conditions as a function of temperature. The error bars are based on at least 48 independent simulations, but those for the isothermal simulations at 4750, 4800 and 4850 K are based on 96 simulations. The solid (red) curves represent simultaneous best fits of both sets of simulation data based on predictions by CNT (a and b) and KNT (c and d).

IV. MELTING OF BULK GRAPHENE

We apply the CNT and KNT described in the previous section to evaluate T_m of a bulk graphene system consisting of N =1008 atoms with PBCs as in Fig. 1. In Fig. 3 we present the results of two sets of systematic MC simulations, including simulations heating the system at a rate η_{MC} and isothermal simulations. In view of the large variations in the respective, observed melting temperature T^*_m and time required for melting, t^*_{MC}, at least 48 independent simulations were performed in all cases, in order to obtain good statistical averages. Best fits to all 13 data points were then determined by using the described CNT and KNT approaches, with fitting parameters K (or $\tilde{K} = \nu_{ref} g$ in the case of KNT), α and T_m. In both cases good agreement was obtained, with estimates for T_m equal to 4450 and 4510 K according to CNT and KNT respectively. This relatively small difference shows that the exponential factor dominates the nucleation rate and that the role of the temperature dependence of the prefactor in KNT is limited. Since KNT is more accurate, we conclude that $T_m \simeq 4510$ K. From α we find $\gamma_{sl} = 0.134$ eV/Å .

V. MELTING OF FINITE GRAPHENE DISKS

Searching for verfication of the result from KNT, we also performed simulations of the melting of a series of roughly circular graphene disks of increasing size. Typically, their melting temperature, $T_{m,d}$, increases as a function of cluster size, as was already demonstrated for small graphene flakes ($N < 55$) in Ref. 19. According to the Pavlov model [20] specified below, $T_{m,d}$ deviates from T_m by a finite size correction that vanishes with the inverse radius of the disk, allowing for the determination of T_m by extrapolation. It should be noticed, however, that the analysis of the disk simulations is arguable because $T_{m,d}$ is not rigorously defined and the Pavlov model does not consider edge melting.

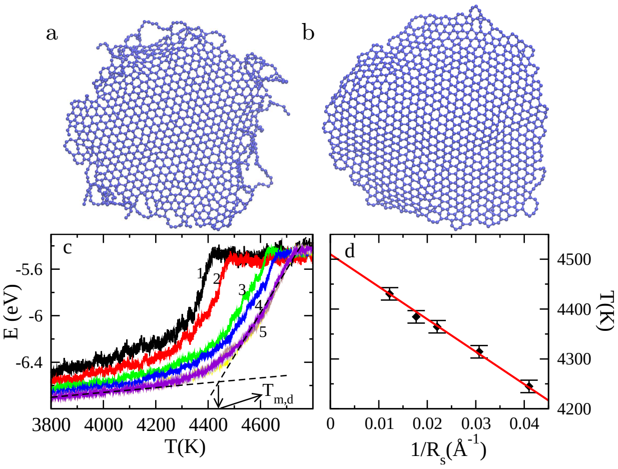

FIG. 4. a) Snapshot at 4300 K, illustrating edge melting of a graphene disk containing 1274 atoms heated at a rate of 2.5 10^{-4} K/cycle. b) Snapshot illustrating the recrystallization after cooling the system in a) from 4300 to 3800 K. c) Melting curves for different graphene disk sizes: 1) 714, 2) 1274, 3) 2470, 4) 3820 and 5) 8020 atoms. For the latter cluster, melting curves from 4 independent simulations are drawn but they are almost overlapping. The crossing dashed lines illustrate the method used to define the melting temperature $T_{m,d}$ of a disk. d) Best fit (red line) according to eq. 7 of the average simulated disk melting temperatures (symbols). The error bars are based on 4 independent simulations.

For a disk, nucleation is not required and the melting starts at the edge, as illustrated in Fig. 4a. According to CNT there is no barrier for nucleation at a 1D edge, which is rough at any T. Therefore there is little variation in $T_{m,d}$ from different simulations, as is illustrated by the almost overlapping melting curves from 4 independent simulations for the cluster with 8020 atoms in Fig 4c.

Interestingly, the melting process is reversible to some extent, as long as there are still solid parts in the system. In Fig. 4b we show the recrystallization that has occurred after the system in Fig. 4a was slowly cooled from 4300 to 3800 K.

An appropriate approach to analyse our simulation data for disks would be a 2D version of Pavlov's model [20]. Writing the free energy of the solid (s) and quasi-2D liquid (l) disk as $G_{d,P} = N_P \mu_P + 2\pi R_P \gamma_{Pv}$ for $P = s, l$, with N_P the number of particles in the solid/liquid disk, R_P their radii and γ_{Pv} the respective edge free energies of their interfaces with the vacuum, and imposing equality of the chemical potentials through $dG_{d,s}/dN_s|_{N_s=N} = dG_{d,l}/dN_l|_{N_l=N}$ leads to the following correction for the melting temperature of a finite disk:

$$T_{m,d} = T_m \left(1 - \frac{\gamma_{sv} - q_\rho \gamma_{lv}}{\rho_s \Delta h R_s}\right) \tag{7}$$

where $q_\rho \equiv (\rho_s/\rho_l)^{1/2}$ accounts for the 2D density difference between solid and liquid.

The results of the disk simulations are summarized in Fig. 4. A clear trend in $T_{m,d}$ as a function of $1/R_s$ is observed and a best fit based on eq. 7 yields $T_m = 4503$ K, a value very close to that derived from KNT, and $\gamma_{sv} - q_\rho \gamma_{lv} = 0.58$ eV/Å . With an (average) value of $\gamma_{sv} \simeq 1.05$ eV/Å for a graphene ribbon from Ref. [21] and taking $q_\rho \simeq 1$ we find $\gamma_{lv} \simeq 0.47$ eV/Å . These edge energies, and also $\gamma_{sl} = 0.134$ eV/Å from KNT reported above, are physically sound, with $\gamma_{sv} > \gamma_{lv} > \gamma_{sl}$.

VI. MELTING OF 2D GRAPHENE RIBBONS

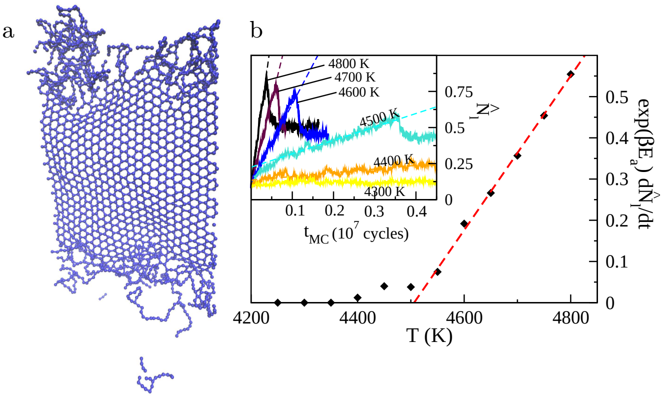

FIG. 5. a) Snapshot of a melting ribbon consisting of 2016 atom at $T = 4500$ K. b) The simulated melting speed (symbols), $\exp(\beta E_a) d\hat{N}_l/dt$, as a function of the temperature T for a graphene ribbon. The inset shows the fraction of liquid particles $\hat{N}_l$ as a function of t_{MC} for various simulation temperatures as indicated. For the completely liquid phase $\hat{N}_l \simeq 0.5$ as many particle still have a $\gamma_{12} < 0.2$ due to a rather isotropic neighbor surrounding.

For further verification of our result for T_m, we have also performed constant temperature melting simulations of a graphene ribbon. We used a ribbon of a size $L_x \times L_y$ = 51.12 × 103.23 Å^2 containing 2016 atoms with PBC only in the x-direction. For this geometry, as for the disks, the melting proceeds from the free edges, as shown in Fig. 5a, and there is no nucleation barrier. In this case of a straight edge, the melting speed, dN_l/dt with N_l the number of liquid particles, which we define as the number of particles with $\gamma_{12} > 0.2$, is expected to behave as $\hat{K}(T)P_{sl}(\exp(-\beta\Delta\mu) - 1)$, where $P_{sl} \simeq 2L_x d/(\pi a^2)$ is the number of sites at the solid-liquid interface and $\hat{K}(T) = (\nu_{ref}T/T_{ref})\exp(-\beta E_a)$. Since $|\beta\Delta\mu| << 1$, the melting speed can be well approximated as:

$$\frac{d\hat{N}_l}{dt} = \frac{\nu_{ref}\Delta h \exp(-\beta E_a)}{k_B T_{ref} T_m} \frac{2L_y d\rho}{N} (T - T_m) \tag{8}$$

where we have defined $\hat{N}_l \equiv N_l/N$ as the fraction of liquid particles. In Fig. 5b we have plotted $\exp(\beta E_a) d\hat{N}_l/dt$ as a function of T obtained from simulations (symbols). The intersection of a best linear fit according to Eq. 8 for $T > 4500$ K with the horizontal axis yields $T_m = 4505$ K, very close to the previously found values. It has to be noticed, however, that the results for $T = 4400$, 4450 and 4500 do not follow the linear law, as the system actually melts for these temperatures. Although finite size effects might play a role here, maybe the most important reason is that chain-like molecular units evaporate from the liquid edges, as illustrated in Fig. 5a. Since equilibrium in the present case is characterized by a liquid edge of fixed average width, evaporation must lead to a thinner and thinner solid core and finally to complete melting. To deal with this issue properly would require to consider a three phase equilibrium. From the simulation results for $T > 4500$ K, using Eq. 8 and the previously found time calibration factor $t = 5.56\ 10^{-4}$ ps/cycle, one can directly determine the attempt frequency ν_{ref}. We find $\nu_{ref} = 2.3\ 10^{14}$ Hz, which is quite reasonable when comparing it to $k_B T_{ref}/h = 0.94\ 10^{14}$ Hz.

VII. SUMMARY AND CONCLUSIONS

By analyzing systematic simulations we have shown that the melting of pristine bulk graphene, a prototype 2D solid embedded in 3D space, follows a two-stage scenario of which the first step from the 2D solid to a quasi-2D liquid phase is well described by nucleation theory for first order phase transitions. As a consequence, graphene has an unambiguously defined bulk melting temperature T_m, found to be 4510 K using the interatomic potential LCBOPII. This value is confirmed by simulations for finite disks and ribbons, which by extrapolation yield T_m's close to that from nucleation theory, and show reversibility to some extent.

Our finding that T_m is higher (about 250 degrees) than for graphite is not likely to be an artifact of LCBOPII. As a qualitative explanation we suggest that the increased stability of graphene is due to a significant positive entropy contribution for the solid phase due to the possibility of relatively large out-of-plane fluctuations (rippling) at low energy costs, as compared to the situation in graphite.

We expect that the melting scenario found for graphene applies to any covalent 2D material. This expectation is supported by recent melting simulations for 2D MoS$_2$, showing coexistence of the 2D solid and liquid phase during melting [22], as we observed for graphene. While measuring T_m for graphene seems to be a real challenge, measurement of T_m becomes easier for 2D material with a (much) lower T_m than that of graphene.

Acknowledgements.The research leading to these results has received funding from the European Union Seventh Framework Programme under grant agreement n604391 Graphene Flagship and from the Foundation for Fundamental Research on Matter (FOM), which is part of the Netherlands Organisation for Scientific Research (NWO). We thank Luca Ghiringhelli for useful discussions.

VIII. APPENDIX: FORMATION ENERGY OF STONE-WALES AND 57 DEFECTS.

A 5775 Stone-Wales (SW) defect can be created in a perfect graphene layer by rotating a single bond by 90 degrees, followed by a geometrical relaxation of the system (see Fig. 6a). It consists of two adjacent 57 defects. By subsequently rotating another appropriate bond by 90 degrees (and relaxing the system), the 5775 SW defects can be split into two 57 defects separated by one pair of hexagons, as shown in Fig. 6b. This process can be repeated to separate the 57 defects more and more, as shown in Fig. 6c and d.

The total formation energy as a function of the separation between the (57) defects according to LCBOPII is given in Fig. 7 and shows that it strongly increases with distance. Similar behaviour was previously reported in Ref. [13], but in that case the 57 defects were created at grain boundaries in a polycrystalline sheet. In the latter work it was shown that the formation energies according to LCBOPII are in very good agreement with those calculated *ab initio* within DFT. The strongly increasing energy implies that the pathway to disorder by the splitting of a SW defects into two 57 defects and their subsequent further diffusion, a scenario in agreement with the KTHNY theory, is very unfavorable. Indeed, we never observed separated 57 defects in our simulations.

[1] A. C. Mitu and A. Z. Patashinskii, Phys. Lett. A 87, 179 (1982); D. R. Nelson, Phys. Rev. B 28, 5515 (1983); M. Kleman, Adv. Phys. 38, 605 (1989); J. F. Sadoc (Editor), Geometry in Condensed Matter Physics (World Scientific, Singapore, 1990); M. I. Katsnelson and A. V. Trefilov, Phys. Met. Metallography 91, 109 (2001); arXiv:cond-mat/9906402; L. Gómez, A. Dobry, Ch. Geuting, H. T. Diep, and L. Burakovsky, Phys. Rev. Lett. 90, 095701 (2003)

[2] M. I. Katsnelson, A. Fasolino, Acc. Chem. Res. **46**, 97-105 (2013).

[3] K. V. Zakharchenko, A. Fasolino, J. H. Los and M. I. Katsnelson J. Phys.: Condens. Matter,**23**, 202202 (2011).

[4] U. Gasser, C. Eisenmann, G. Maret, P. Keim, ChemPhysChem **11**, 963 (2010).

[5] J. M. Kosterlitz, D. J. Thouless, J. Phys. C **6**,1181 (1973).

[6] B. I. Halperin, D. R. Nelson, Phys. Rev. Lett **41**, 121 (1978).

[7] D. R. Nelson, B. I. Halperin Rev. B **19**, 2457 (1979).

[8] A. P. Young Phys. Rev. B **19**, 1855 (1979).

[9] K. Chen, T. Kaplan and M. Mostoller, Phys. Rev. Lett. **74**, 4019 (1995).

[10] G. Blatter, M. V. Feigel'man, V. B. Geshkenbein, A. I. Larkin, and V. M. Vinokur, Rev. Mod. Phys. **66**, 1125 (1994).

[11] A. Fasolino, J. H. Los, M.I. Katsnelson, Nat. Mater. **6**, 858 (2007).

[12] J. Coraux, A. T. N'Diaye, C. Busse, T. Michely, Nano Lett. **8**, 565 (2008).

[13] J. M. Carlsson, L. M. Ghiringhelli, A. Fasolino, Phys. Rev. B **84**, 165423 (2011).

[14] J. H. Los, L. M. Ghiringhelli, E. J. Meijer, A. Fasolino, Phys. Rev. B **72**, 214102 (2005); **73**, 229901(E) (2006).

[15] V. M. Bedanov, G. V. Gadyak and Yu E. Lozovik, Phys. Lett. A **109**, 289 (1985).

[16] F. Colonna, J. H. Los, A. Fasolino, E. J. Meijer, Phys. Rev. B 80, 134103 (2009).

[17] D. Kashchiev, Nucleation: Basic Theory and Applications (Butterworth-Heinemann, Oxford, 2000).

[18] Huitema, H. E. A., van der Eerden, J. P., J. Chem. Phys. 110, 3267 (1999).

[19] S. K. Singh, M. Neek-Amal, and F. M. Peeters Phys. Rev. B **87**, 134103 (2013).

[20] P. Pavlov, Z. Phys. Chem., Stoechiom. Verwandtschaftsl.**65**, 1 (1909);**65**, 545 (1909).

[21] J. M. H. Kroes, M. A. Akhukov, J. H. Los, N. Pineau, and A. Fasolino, Phys. Rev. B **83**, 165411 (2011).

[22] S. K. Singh, M. Neek-Amal, S. Costamagna and F. M. Peeters, arXiv:1412.1939.

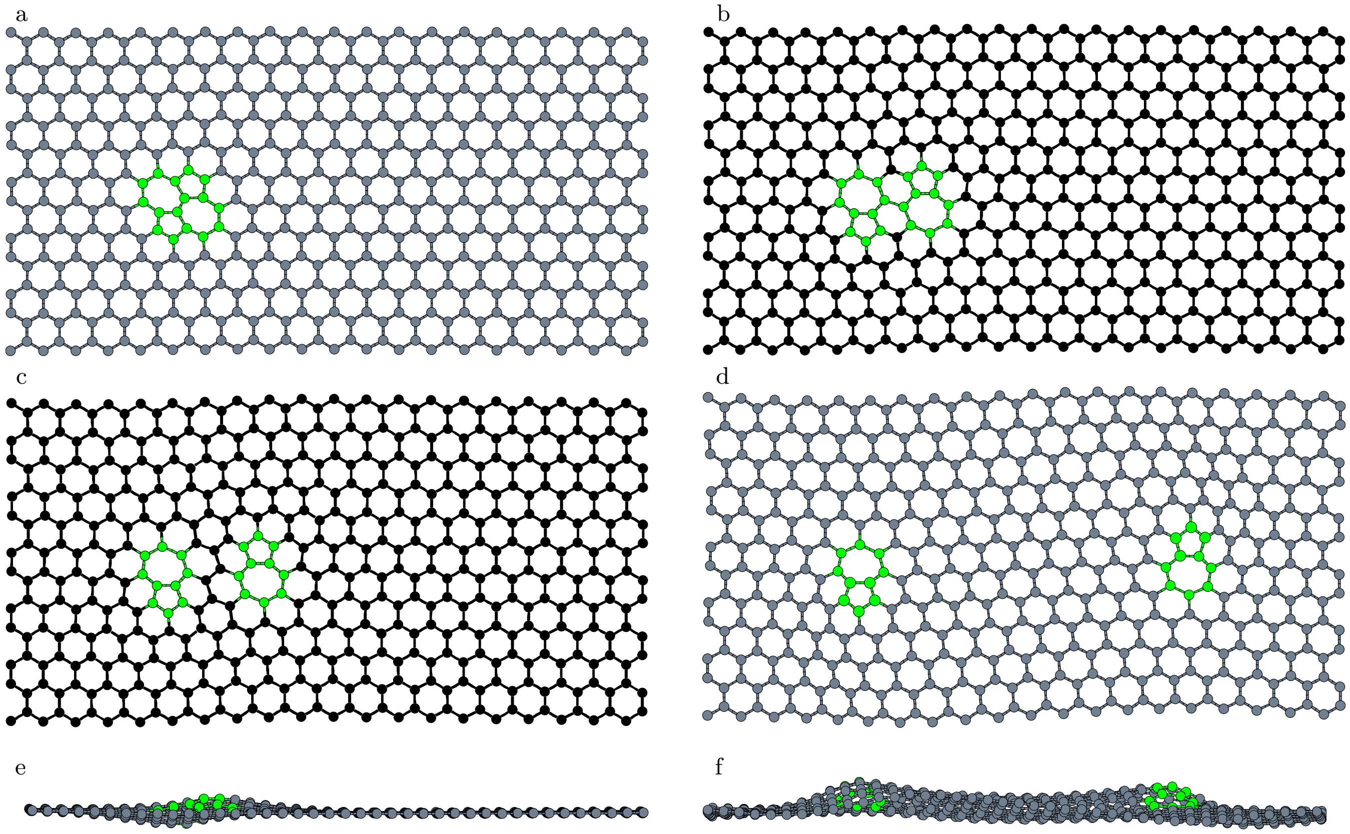

FIG. 6. Step by step separation of the 5775 SW defect (a) into two 57 defects with one (b), two (c) and nine (d) hexagonon pairs in between. Panels e) and f) are side views of the configuration in a) and d), showing much larger out-of-plane deformations for the case of separated 57 defects, due to strong stress in that case.

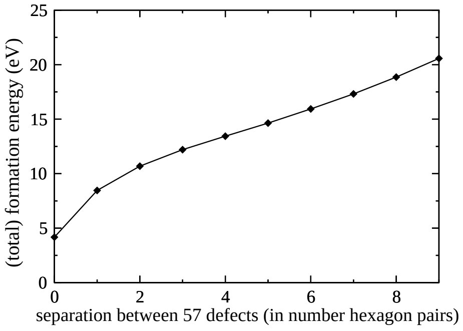

FIG. 7. Total formation energy as a function of the separation between 57 defects according to LCBOPII, calculated for the same sample as used for Fig.6